Direct Reaction Field Force Field: A Consistent Way to Connect and Combine Quantum-Chemical and Classical Descriptions of Molecules

PIET TH. VAN DUIJNEN* AND ALEX H. DE VRIES†

Organic and Molecular Inorganic Chemistry (OMAC), State University of Groningen, Nijenborgh 4, 9747 AG Groningen, The Netherlands: e-mail for P.T.V.D.: ptvd@chem.rug.nl

Received August 18, 1995; revised manuscript received November 17, 1995; accepted November 17, 1995

ABSTRACT

The direct reaction field (DRF) force field gives a classical description of intermolecular interactions based on ab initio quantum-chemical descriptions of matter. The parameters of the DRF force field model molecular electrostatic and response properties, which are represented by distributed charges and dipole polarizabilities. The advantage of the DRF force field is that it can be combined transparently with quantum-chemical descriptions of a part of a large system, such as a molecule in solution or an active site in a protein. In this study, the theoretical basis for the derivation of the parameters is reviewed, paying special attention to the four interaction components: electrostatic, induction, dispersion, and repulsion. The ability of the force field to provide reliable intermolecular interactions is assessed, both in its mixed quantum-chemical–classical and fully classical usage. Specifically, the description of the water dimer and the solvation of water in water is scrutinized and seen to perform well. The force field is also applied to systems of a very different nature, viz. the benzene dimer and substituted-benzene dimers, as well as the acetonitrile and tetrachloromethane dimers. Finally, the solvation of a number of polar solutes in water is investigated. It is found that as far as the interaction energy is concerned, the DRF force field provides a reliable embedding scheme for molecular environments. The calculation of thermodynamic properties, such as solvation energy, requires better sampling of phase space than applied here.

* To whom correspondence should be addressed.
† Present address: Daresbury Laboratory, Daresbury, Warrington, Cheshire WA4 4AD, United Kingdom.

International Journal of Quantum Chemistry, Vol. 60, 1111–1132 (1996)

CCC 0020-7608 / 96 / 061111-22

Introduction

The direct reaction field (DRF) approach to the description of the condensed phase provides a consistent route from a quantum-chemical to an all-classical force-field calculation of intermolecular interactions, at the same time allowing combination of quantum-chemical, discrete classical, and continuum description of various parts of condensed-phase systems, as illustrated in Figure 1 [1–9]. The transition is based on the perturbation-theoretical analysis of the interaction energy in terms of molecular electrostatic and response properties [10–12]. The attraction of modeling molecular properties in this setting is twofold. First, the description may be systematically improved according to the required accuracy. The approach shares this aspect with ab initio quantum chemistry which allows larger basis-set and configuration state function expansions with eventual convergence to exact results. Second, the theoretical analysis provides a check on the validity of the classical model, which makes it easy to pinpoint those parts of the force field that need reparation if things go wrong, without rendering other parts of the parameterization obsolete.

The molecular properties of interest for the calculation of intermolecular interactions are the electrostatic multipole (charge, dipole, quadrupole, etc.) and response moments (dipole polarizability and higher-order response moments). These may be modeled in various ways and to certain degrees of sophistication. The choices—it is important to stress these are choices!—made in this work for distributed representations of both static and response moments, and for stopping at the exact representation of the overall dipole moment [13] and at linear response [14] have been described [9]. Here we test the model both against internal consistency as we go from a fully quantum-chemical through a mixed to a fully classical description of molecular dimers and against experimental data. The latter is important for estimating the reliability of interaction energies of molecular complexes predicted by the classical force field.

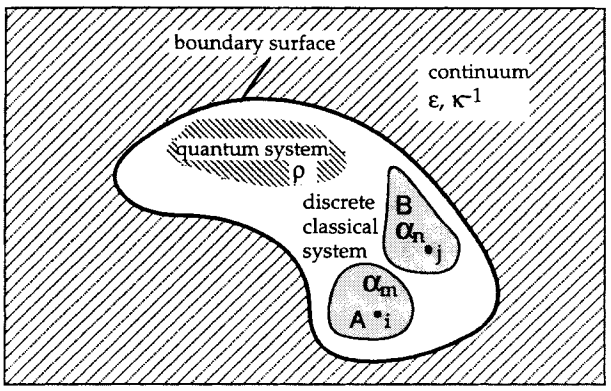

FIGURE 1. General condensed-phase model.

The interaction energy between two molecules is analyzed in the following terms, be it for quantum-chemical, mixed, or classical descriptions:

$$\Delta U_{\text{int}} = \Delta U_{\text{elst}}^{\text{int}} + \Delta U_{\text{rep}}^{\text{int}} + \Delta U_{\text{resp}}^{\text{int}} + \Delta U_{\text{disp}}^{\text{int}} \quad (1)$$

or electrostatic, repulsion, response, and dispersion. This analysis is straightforward for the classical and mixed descriptions, but contains elements of arbitrariness at small intermolecular distances for the quantum-chemical approach because of the inseparability of the total wave function into fragment functions. At larger intermolecualr distances there is no problem; the fragments are recognizable and nonoverlapping.

As soon as the fragment wave functions start overlapping, the integrity of the fragments is violated and analysis becomes cumbersome [10, 11, 15]. Straightforward analysis starts with calculation of the total energy—in the Hartree–Fock approximation, accounting for basis-set superposition errors by the counterpoise method [16, 17]—of the molecular complex by superimposing the fragment densities, U_{A+S}^{HF}. The energy difference of U_{A+S}^{HF} with the sum of the isolated fragment energies is the electrostatic interaction energy if the fragments are nonoverlapping. If the fragment wave functions do overlap, the superimposed state is unphysical, however, because it then violates the Pauli principle. The first physically meaningful interaction energy can be defined only after this principle has been implemented by orthogonalizing the fragment wave functions," contributing $\Delta U_{\text{orth}}^{\text{HF}}$. Thus, in a fully quantum-chemical treatment, the electrostatic and repulsion terms are best collected, and denoted ΔU_1:

$$\Delta U_1 = U_{A+S}^{\text{HF}} - (U_A^{\text{HF}} + U_S^{\text{HF}}) + \Delta U_{\text{orth}}^{\text{HF}} \cong \Delta U_{\text{elst}} + \Delta U_{\text{rep}}. \quad (2)$$

At large intermolecular distances the orthogonalization has no effect, so that it is meaningful to

use the superimposed state to define the electrostatic interaction energy.

From the orthogonalized state the fragment wave functions may be allowed to relax to accommodate their mutual influence. The energy difference between the fully relaxed state and the orthogonalized state is the response contribution to the interaction energy. At smaller intermolecular distances the relaxation of the wave function may aggravate the problem of dealing in terms of recognizable fragments as chemical bonding starts to become important. One may still attempt to analyze the contributions in terms of fragments by localizing the orbitals as much as possible, ascribing each orbital to a fragment according to its character. The resulting energy analysis is somewhat arbitrary because there are many different localization schemes. Good localization is even more important for the calculation of the dispersion interaction. This interaction is not included at the Hartree–Fock level, which lacks the instantaneous electron–electron interactions that define the dispersion. Calculation at a correlated level includes the dispersion interaction which may, however, only be analyzed as such if properly localized occupied as well as virtual fragment orbitals are available. Again, this requirement is easily fulfilled at large intermolecular distances, but no longer as the fragments start overlapping. For weakly interacting systems (including the water dimer) the dependence on the localization was found to have little effect on the analysis, though [18].

The most fruitful and physically viable approach is then to maintain the long-range analysis as much as possible, bearing in mind the invalidity of the transition from quantum-chemical to mixed and classical descriptions as the intermolecular separation becomes small. It is allowable, however, to stretch the classical model a bit by accounting for overlap effects. At intermediate intermolecular separations quantum-chemical results may yield good models for damping functions which account for the spatial extent of the fragment electronic density within a classical description. The advantage of the classical representation of the charge density lies in the drastic reduction of detail by using just a small number of charge points instead of the large number of basis functions covering large parts of space used in quantum-chemical methods. The neglect of the spatial extent of the charge distribution by the charge-point representation may be repaired without too much computational effort by assuming the charge to be distributed in simple volumes, instead of being concentrated in one point in space. Thole has investigated several of these volumes with their shape functions and found them to be useful even at typical *intramolecular* interatomic distances [14].

Having constructed a molecular force field based on the long-range interaction energy analysis, and maintaining it with plausible damping functions at intermediate distances, the task of avoiding flagrant violation of the Pauli principle by some ad hoc repulsive interaction function remains. Ideally, one would like a functional form that puts a high penalty on the penetration of the electrons treated explicitly into the regions of space that are already claimed by the electrons that underlie classically modeled molecules. Such functional forms do exist, but are computationally highly demanding because they are almost at the level of the original quantum-chemical description itself [19–23]. (To add to the complexity of this task, the effective potentials should not neglect the give-and-take character of the antisymmetrization in the valence region.) Indeed it is hardly to be expected that such a far-reaching requirement as the antisymmetry due to the Pauli principle can be modeled by a simple functional form. For the molecular systems of interest in describing van der Waals dimers and condensed-phase systems such an elaborate procedure would miss its mark, because the basic assumption for using the molecular model is the non- or low overlap of the molecular fragments. If, however, bonds are to be cut in the separation of quantum and classical fragments, the development of effective fragment potentials is essential.

The ad hoc repulsive potential chosen here is taken from the existing CHARMM force field [24], albeit with slightly different values of the parameters in order to converge on the other parts of the DRF force field. The CHARMM repulsion has the form:

$$\Delta U_{\text{rep}}^{\text{CHARMM}} = \sum_{i<j} \frac{3}{4} \frac{\alpha_i \alpha_j (r_i + r_j)^6}{\left(\sqrt{\alpha_i/n_i} + \sqrt{\alpha_j/n_j}\right)} r_{ij}^{-12} \quad (3)$$

in which α_i, n_i, and r_i are the isotropic polarizability, number of valence electrons, and radius of atomic center i, respectively, and r_{ij} is the distance between centers i and j. We use the integral number of valence electrons of an atom, and the same atomic polarizabilities that go into the elec-

trostatic (for the damping function), response, and dispersion terms, leaving only the atomic radii as independent parameters to be optimized. By noting that the radius of an atom may be related to its polarizability—classically, the polarizability of a conducting sphere of radius r equals r^3—the number of parameters can be reduced further. Theoretically, the repulsion term should have exponential distance dependence [10], and the 12-type repulsion model is known to be too steeply repulsive at shorter contacts. We note again that the repulsion serves to avoid situations that can only be described properly by a fully quantum-chemical treatment.

The estimate of the dispersion interaction between a quantum-chemically described molecule A and a classically described molecule S emerges from the comparison of the second-order perturbation (SOP) expression in the Unsöld approximation to the two-electron reaction-field contributions to the total energy [1, 3, 25]. In a fully quantum-chemical description the SOP expression for the dispersion interaction between A and S is given by:

$$\Delta U_{\mathrm{SOP}}^{\mathrm{disp}} = \sum_{k,m\neq 0} \frac{\left|\langle \Psi_A^0 \Psi_S^0 | \hat{V}_{AS} | \Psi_A^k \Psi_S^m \rangle\right|^2}{U_{A,0} - U_{A,k} + U_{S,0} - U_{S,m}}$$

with $\hat{V}_{AS}$ the intersystem interaction Hamiltonian, and $U_{X,m}$ the energy of system X in its mth state. In the long-range approximation the integrations in A and S may be separated, while one center expansions up to the dipole terms for the interaction leads to:

$$\Delta U_{\mathrm{SOP}}^{\mathrm{disp}} \approx \sum_{k,m\neq 0} \frac{\left|\langle \Psi_A^0 | \hat{\mathbb{E}}_\mu(\mathbf{s};\mathbf{a}) \hat{\mu}_A \hat{\mathbb{E}}_\mu(\mathbf{s};\mathbf{a}) | \Psi_A^k \rangle\right|^2 \times \left|\langle \Psi_S^0 | \hat{\mu}_S | \Psi_S^k \rangle\right|^2}{(U_{A,0} - U_{A,k}) + (U_{S,0} - U_{S,m})} \tag{4}$$

in which $\hat{\mathbb{E}}_\mu(\mathbf{s};\mathbf{a})$ is the operator that gives the field at $\mathbf{r}_a^0$ of a dipole located at $\mathbf{r}_s^0$:

$$\hat{\mathbb{E}}_\mu(\mathbf{s};\mathbf{a}) = \hat{\mathbb{E}}_\mu(\mathbf{r}_s^0;\mathbf{r}_a^0) = \frac{1}{|\mathbf{r}_a^0 - \mathbf{r}_s^0|^3}\left\{\mathbb{I} - \frac{3(\mathbf{r}_a^0 - \mathbf{r}_s^0)(\mathbf{r}_a^0 - \mathbf{r}_s^0)^\dagger}{|\mathbf{r}_a^0 - \mathbf{r}_s^0|^2}\right\} \tag{5}$$

and $\hat{\mu}_A$ and $\hat{\mu}_S$ are the dipole operators of subsystems A and S, respectively.

Equation (4) can be expressed in terms of the polarizabilities of the subsystems by invoking the Unsöld approximation that enables a splitting of the denominator:

$$\frac{1}{U_{A,0} - U_{A,k} + U_{S,0} - U_{S,m}} = \frac{\overline{U}_A \overline{U}_S}{\overline{U}_A + \overline{U}_S} \frac{1}{(U_{A,k} - U_{A,0})(U_{S,m} - U_{S,0})}\{1+\Delta\};$$

$$\Delta = \frac{\frac{1}{\overline{U}_A} - \frac{1}{U_{A,0} - U_{A,k}} + \frac{1}{\overline{U}_S} - \frac{1}{U_{S,0} - U_{S,m}}}{(U_{A,0} - U_{A,k})^{-1} + (U_{S,0} - U_{S,m})^{-1}} \tag{6}$$

in which $\overline{U}_A$ and $\overline{U}_S$ are chosen to minimize Δ. It is seen that the error Δ is small as long as $\overline{U}_A$ and $\overline{U}_S$ do not deviate too much from the individual excitation energies. Inserting eq. (6) into eq. (5), the polarizabilities of A and S are recognized, leading to the approximate dispersion interaction expression:

$$\Delta U_{\mathrm{SOP}}^{\mathrm{disp}} \approx -\frac{1}{2}\frac{U_S}{U_A + U_S} \sum_{k\neq 0} \langle \Psi_A^k | \hat{\mathbb{E}}_\mu(\mathbf{s};\mathbf{a}) \hat{\mu}_A | \Psi_A^0 \rangle^\dagger \times \alpha_S \langle \Psi_A^k | \hat{\mathbb{E}}_\mu^\dagger(\mathbf{s};\mathbf{a}) \hat{\mu}_A | \Psi_A^0 \rangle. \tag{7}$$

In Eq. (7) the polarizability of S is inserted, but the sum-over-states expression for A is retained. Addition and subtraction of the $k = 0$ term to Eq. (6) yields a fluctuation formula for the dispersion:

$$\Delta U_{\mathrm{SOP}}^{\mathrm{disp}} \approx -\frac{U_S}{U_A + U_S} \times \begin{Bmatrix} \frac{1}{2}\langle \Psi_A^0 | [\hat{\mathbb{E}}_\mu(\mathbf{s};\mathbf{a})\hat{\mu}_A]^\dagger \alpha_S \hat{\mathbb{E}}_\mu(\mathbf{s};\mathbf{a})\hat{\mu}_A | \Psi_A^0 \rangle \\ -\frac{1}{2}\langle \Psi_A^0 | [\hat{\mathbb{E}}_\mu(\mathbf{s};\mathbf{a})\hat{\mu}_A] | \Psi_A^0 \rangle^\dagger \alpha_S \langle \Psi_A^0 | \hat{\mathbb{E}}_\mu(\mathbf{s};\mathbf{a})\hat{\mu}_A | \Psi_A^0 \rangle \end{Bmatrix}. \tag{8}$$

Now a transition to a mixed description can be made by modeling the polarizability of subsystem S clasically. The DRF operator

$$\hat{H}_{\mathrm{DRF}} = -\frac{1}{2}\sum_{i,j\in A} \hat{E}_{AS}^\dagger(i)\alpha_S \hat{E}_{AS}(j) \tag{9}$$

expresses the influence of a polarizable environment S on a quantum-mechanically described system A. Here $\hat{E}_{AS}$ is the field-operator of A at S. One may read this formula as follows: The charges in A exert a field at S, and induce a dipole proportional to the field and the polarizability at

S; the resulting dipole in turn exerts a potential at the charges in A. Both terms within the rightmost brackets in Eq. (8) are computed within the DRF approach, but note that the DRF operator [Eq. (9)] is not restricted to the one center dipole term, and that α_S is not necessarily a single-point polarizability [9]. The difference between the two terms in Eq. (8) is the instantaneous versus average coupling of the quantum system to the reaction field. The prefactor $U_S/(U_A + U_S)$ is not present in the expectation values of the DRF operator and is left as a scaling between the SOP estimate and the computed DRF value. In most applications the ionization energies of the molecules A and S have been used to calculate the prefactor. If A and S are identical, the prefactor, called γ, equals 0.5.

To complete the journey from fully quantum-chemical through the mixed to the fully classical description, the dispersion between clasically described molecules is given by the Slater–Kirkwood version of the SOP expression [26], expressing the prefactor in terms of the polarizability (again!) and number of valence electrons, rather than excitation energies, as in the mixed [Eq. (8)] and classical London dispersion formulas:

$$\Delta U_{\text{disp}}^{S-K} = -\sum_{i<j} \frac{1}{4} \frac{\text{Tr}\left(\alpha_i \hat{\mathbb{E}}_{\mu ij}^2 \alpha_j\right)}{\left(\sqrt{\alpha_i/n_i} + \sqrt{\alpha_j/n_j}\right)}. \quad (10)$$

The summation may be over atomic or group polarizabilities, which may be treated as isotropic or anisotropic, according to the polarizability representation of choice.

The Water Dimer

The water dimer fulfills the role for force fields that the hydrogen molecule fulfills for the representation of the chemical bond and the helium dimer for the accurate calculation of intermolecular interactions. The literature abounds with water–water potentials to varying degrees of accuracy, derived from quantum-chemical computations and from experimental data and from mixtures [6, 27–37]. Aspects of the water model presented here have been discussed before. Here, the exposition aims at demonstrating the derivation of the classical force field from quantum-chemical calculations. The extensive quantum-chemical studies of the water-dimer potential energy surface (PES) of Jeziorski and Hemert (I) [38], Vos et al. (II) [18], and Szalewicz et al. (III) [39] serve as our reference, together with the accurate calculation of the well-depth at the minimum-energy conformation of van Duijneveldt-van de Rijdt and van Duijneveldt (III) [40]. A comprehensive review of the water–water interaction by ab initio methods was published by Scheiner [41]. The molecular electrostatic properties of water in our model are derived from the RHF wave function with a basis set of double-ζ quality in the valence shell plus a polarization function (DZP) [42]. The comparison is therefore with literature results of similar quality. Finally we proceed to comparison to experimental results [43] in order to test the model for its potential to predict binding energies of molecular complexes.

COMPARISON TO ab initio RESULTS

The computed water dipole and quadrupole moments and dipole polarizability are collected in Table I, together with the values of these properties given by the classical model. The classical model consists of three point charges and three atomic polarizabilities located at the nuclei. The point charges are the dipole preserving charges (DPCs) by Thole and van Duijnen [13]. The atomic polarizabilities were chosen to reproduce the computed polarizability within Thole's model [14]. (The standard polarizabilities in Thole's model reproduce experimental molecular polarizabilities, a standard computations the DZP level cannot attain.) Two shape functions were studied, corresponding to a linearly (LIN) and an exponentially (EXP) decaying volume for the charge, respectively. It is not yet our aim to reproduce experimental values, so the values in Table I serve to illustrate the correspondence between quantum-chemical and classical model properties.

The interaction components of the water dimer were studied in the orientation of the experimental water–dimer minimum-energy conformation [43], shown in Figure 2. The quantum-mechanical (QM) water was treated both as H-bond donor and as H-bond acceptor in order to investigate the orientation dependence of the mixed description. The comparisons of the first-order, relaxation, and dispersion components of the interaction energy of the water dimer as a function of O–O distance are shown pictorially in Figure 3–5. Only the results for the exponential damping function are shown here. At O–O distances above 6 bohrs, the results for the linear damping function are virtually identical to those obtained with the exponential damp-

TABLE I
Water properties[a] from ab initio calculations and classical models.

Model	μ_x	Θ_{xx}	Θ_{yy}	Θ_{zz}	α_{xx}	α_{yy}	α_{zz}
DZP (CHF)[b]	0.878	−0.08	1.82	−1.74	5.42	7.18	3.03
DZP (SOP)[c]					5.50	6.65	3.53
LIN[d,e]	0.878	−0.06	1.26	−1.19	4.95	6.97	3.66
EXP[d,f]	0.878	−0.06	1.26	−1.19	5.12	6.31	4.28
exp.[g]	0.728	−0.10	1.96	−1.86	9.5	9.7	9.2

[a] All values in atomic units. The tensor components not given all equal zero in the geometry studied.
[b] Polarizability from coupled Hartree–Fock calculation.
[c] Polarizability from second-order perturbation calculation with nonempirical Unsöld correction for finite basis-set size (Ref. [44]).
[d] Atomic charges: O, −0.796; H, +0.398.
[e] Atomic polarizabilities: O, 2.417; H, 1.442, damping parameter a = 1.662 with conical charge volume (Ref. [14]).
[f] Atomic polarizabilities: O, 2.666; H, 1.448, damping parameter a = 2.089 with exponentially decaying charge volume (Ref. [14]).
[g] Experimental water properties. Dipole from Ref. [45]; quadrupole from Ref. [46]; semi-empirical polarizability from Ref. [47].

ing function. As the monomers close in, the linear damping function does not behave as smoothly as the exponential one. Instead, it results in a deeper and narrower potential well.

Bearing in mind that at room temperature RT corresponds to 2.5 kJ/mol, Figures 3–5 show that the interaction-energy components in the mixed and classical descriptions start deviating seriously from the ab initio results only at intermolecular distances shorter than 5.5 bohrs, where the relaxation and dispersion energies differ notably from the fully QM results, pointing to an overdamping of the classical model. This overdamping can be repaired, but in the mixed model this might lead to the polarization catastrophe for the linear damping model. Furthermore, one should not expect the classical model to be satisfactory well inside the overlap region, where typically quantum-chemical effects due to the operation of the Pauli principle govern the distribution of the electrons. Another feature worth some attention is the orientation dependence of the interaction components in the mixed description. This was already noted by Thole and van Duijnen [3] and reflects an imbalance in the distributed charge and polarizability representations used. The problem is mainly due to the short H–O distance due to hydrogen bonding. Hence, the relaxation energy of the QM H-bond donor is larger than that of the QM H-bond acceptor because the donor molecule "sees" a large charge on O quite nearby, whereas the acceptor sees a small charge on H, to which the vacuum densities respond accordingly. On the other hand, the dispersion interaction is larger for the QM H-bond acceptor because there are some eight electrons "seeing" a H polarizability, compared to about one electron seeing an O polarizability, which is not even twice that of H. The imbalance vanishes as the distance between the molecules increase, as it should when local effects disappear.

The imbalance can be repaired for the dispersion by using a group-polarizability representa-

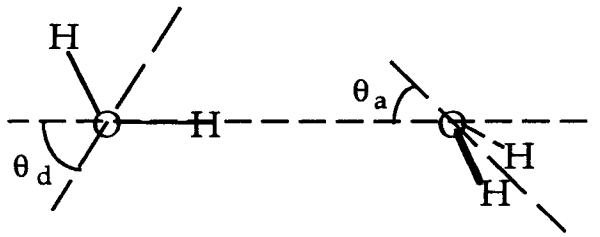

FIGURE 2. Experimental water-dimer orientation. θ_d = 51°; θ_a = 57°.

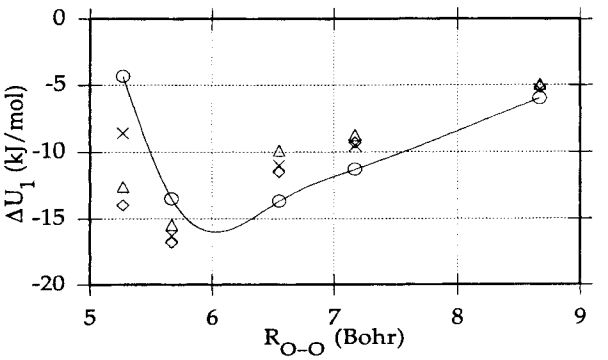

FIGURE 3. Comparison of the zeroth-order interaction energy of the water dimer in various descriptions, as a function of O–O distance. (○) fully QM description; (△) mixed description with QM water as H-bond donor; (◇) mixed description with QM water as H-bond acceptor; (×) fully classical description.

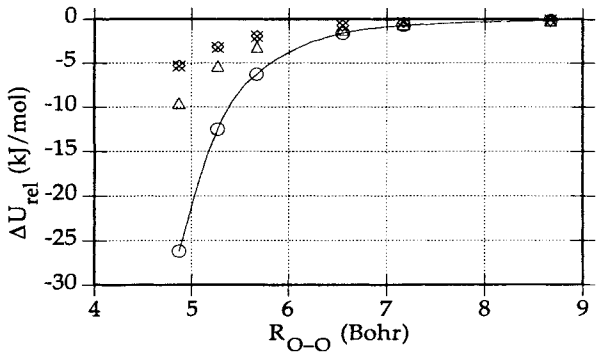

FIGURE 4. Comparison of the relaxation energy of the water dimer in various descriptions, as a function of O–O distance. (○) fully QM description; (△) mixed description with QM water as H-bond donor; (◇) mixed description with QM water as H-bond acceptor; (×) fully classical description.

tion. The group polarizability will be located quite near the O atom, hardly changing things for the QM H-bond donor, but causing a drop in the dispersion interaction for the QM H-bond acceptor because of the increased distance of the polarizability to the acceptor O.

Finally, suffice it to conclude that the fully quantum-chemical, mixed, and fully classical models are compatible at long and intermediate intermolecular distances. The fact that even the H-bonded water dimer is accommodated quite well within this model demonstrates its scope. Thus we expect to be able to predict van der Waals minima of ab initio quality with the classical model for molecular complexes of molecules other than water. This may not be good enough, however, for

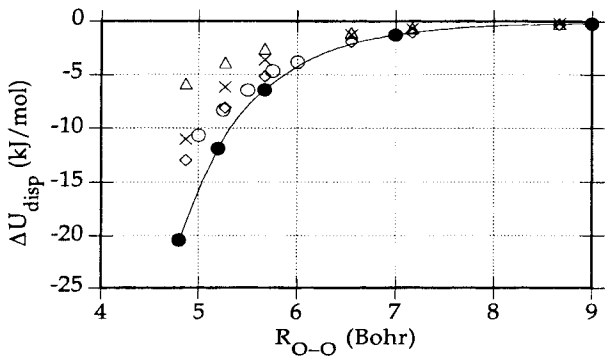

FIGURE 5. Comparison of the dispersion energy of the water dimer in various descriptions, as a function of O–O distance. (○) fully QM description I; (●) fully QM descirption (II; (△) mixed description with QM water as H-bond donor; (◇) mixed description with QM water as H-bond acceptor; (×) fully classical description.

practical purposes which are geared to the prediction of experimental interaction energies. The improvements required for attaining experimental standards are the subject of the next section.

COMPARISON TO EXPERIMENTAL RESULTS

The DZP-derived classical model polarizability of water is rather small compared to experiment (see Table I), resulting in an underestimation of the induction and dispersion interaction energies compared to accurate calculations. If the model is to be used to yield interaction energies comparable to experimental values, the polarizability is the prime candidate for improvement. Of course, correlated large basis-set calculations [48] could be invoked to calculate molecular polarizabilities that can then be reproduced by Thole's model. The standard atomic polarizabilities of Thole's model do, however, yield molecular ground-state polarizabilities of experimental quality for molecules outside the learning set, disposing of the immediate need to perform costly ab initio calculations. (For excited states there is a call for such calculations [49] because of the limited availability of experimentally determined polarizabilities [49, 50].) For instance, water was not in Thole's learning set but its experimental polarizability is reproduced quite well by the model (parameters are given in Appendix 1). With the group polarizability thus obtained, the total interaction energy curve of the water dimer was recalculated in the mixed and classical descriptions, and is shown in Figure 6.

The agreement between the standard DRF force field and high-quality ab initio calculations for both mixed and fully classical descriptions is excellent at the minimum. In this discussion it must be borne in mind that the minimum energy by van Duijneveldt-van de Rijdt and van Duijneveldt (IV) should be regarded as the best available value, comparing very well to experiment after thermodynamic corrections. The deeper wells obtained earlier (I and III) are mostly due to the dispersion contribution, which was shown to be sensitive to the exponent of the polarization function [40]. The short-range interaction is too repulsive, in accord with the exaggerated steepness of the 12-type repulsion term. Reparation of the dipole polarizability of the water monomers provides the major correction to the DZP-level results. Further sophistication of the description of the monomer properties is not deemed necessary for the purposes pursued here. For calculation of, e.g., rotation–

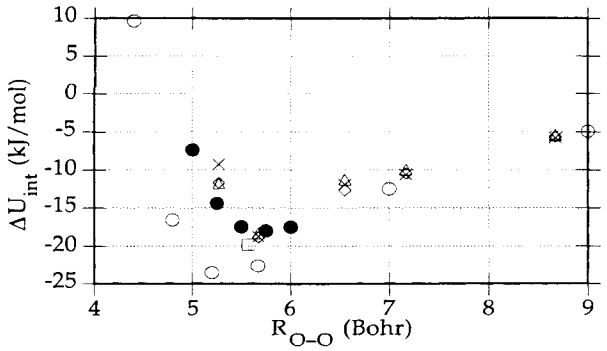

FIGURE 6. Comparison of the total interaction energy of the water dimer in various descriptions, as a function of O–O distance. (○) fully QM description I; (●) fully QM description II; (□) estimated ab initio limit (QM IV); (△) mixed description with QM water as H-bond donor; (◇) mixed description with QM water as H-bond acceptor; (×) fully classical description.

vibration spectra the DRF scheme is too crude. The small splittings encountered there require accurate description of higher-order molecular properties [51]. We conclude that the transition from (accurate) ab initio QM descriptions through mixed to the fully classical DRF force field is very satisfactory for the calculation of intermolecular interaction energies as long as we keep in mind that the approach is bound to break down at intermolecular distances that enter the region of covalency.

Complexes of Benzene and Its Derivatives

The benzene dimer has been regarded as a prototype for the study of π–π interactions in (macro)molecular complexes and in proteins [52, 53]. The observed preference for parallel-displaced (I, II) and perpendicular (III, IV) over parallel-sacked orientations (see Fig. 7) in these compounds has been ascribed to the electrostatic interaction between the π systems. The repulsion of the electron charge clouds above and below the molecular plane of π systems dominates in the parallel orientation, whereas in the perpendicular and displaced orientations the overall electrostatic interaction is favorable. The main contribution to the *binding energy* of the benzene dimer is, however, not from the electrostatic but from the dispersion interaction. The dispersion is claimed to be hardly orientation dependent [52, 54] and thus not to prefer a particular intermolecular structure.

The leading electrostatic moment of benzene is the quadrupole. In proteins phenyl rings are always attached to the backbone, introducing a possibly large dipole moment which may dominate the electrostatic interaction with the surroundings. If the phenyl rings are further substituted with, e.g., hydroxyl groups, the dipole moment becomes even more prominent. The study of benzene derivative, such as toluene, xylene, and fluorobenzene, is expected to shed light on the consequences of the substitution of phenyl rings on interaction energy and conformation. Molecular beam experiments on clustering have been performed on some benzene derivatives, both of the pure substance and of mixtures [55]. For the interpretation of these experiments a number of parameters are required that are not all that easy to determine independently, one of them being the binding energy. The experimental determination of the binding energy is quite difficult [56–58] and accurate calculation is therefore warranted as a check on the experiments [54, 59].

Accurate computation of dispersion interactions requires excellent description of the molecular

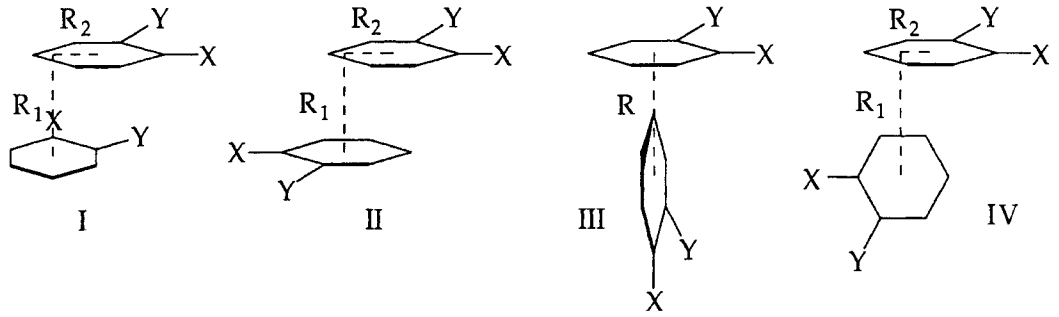

FIGURE 7. Substituted-benzene dimer conformations. (I) parallel-displaced; (II) anti-parallel-displaced; (III) head-on perpendicular; (IV) side-on perpendicular.

electronic spectrum, which can only be done by using both large one-electron and large configuration basis-set expansions in current ab initio methods. Only very few such studies have been published. The problem with the arenes is that they are planar, but an important portion of their electron density resides outside the plane. Standard one-electron basis-set expansions tie their basis functions to the nuclei, and provide insufficient opportunity for the electrons to distribute themselves in the regions above and below the molecular plane. This deficiency may be repaired only at great costs as the computational effort grows with the sixth power of the number of basis functions. Reliable (semi-)empirical models for the computation of the dispersion interaction in molecular complexes are therefore very valuable to supplement state-of-the-art quantum chemistry.

The DRF force field provides a fairly good estimate of the dispersion interaction because experimental molecular polarizabilities are represented very well by Thole's model. Although the interaction energy gained by going beyond the Hartree–Fock level in ab initio treatments includes more than just the dispersion connected to the dipole polarizabilities, the major contribution is captured by the DRF model for the water dimer. Here we investigate a number of molecular arene complexes, starting with the benzene dimer. The standard all-classical DRF force field is shown to agree on the binding energy and preferred orientation with the best ab initio study published for this dimer.

THE BENZENE DIMER

The benzene dimer potential has been studied extensively [54, 60–63]. Accurate ab initio calculations are sparse, the best published by Hobza et al. [54], who find a parallel-displaced conformation (I) to be slightly more stable than a head-on perpendicular one (III). From experimental determination of the principal moments of inertia, the preferred orientation of the benzene molecules was found to be slightly tilted away from being perpendicular [64, 65]. The experiment reflects the thermodynamic average of all possible conformations, and it is to be expected that perpendicular conformations are more numerous than parallel-displaced ones, outweighing them in the thermodynamic average.

The minimum-energy conformations found by Hobza et al. [54] were studied with our all-classical DRF force field. Dipole preserving charges (DPCs) located at the nuclei only were derived from a HF-level calculation in a basis of STO4-31G quality. These do not fully reproduce the experimental quadrupole moment, although better than those obtained from a DZP-quality HF wave function, as can be seen from Table II in which computed and experimental molecular properties are collected. Two other sets of charges that do reproduce the quadrupole moment were investigated as well. The first set is obtained by simply scaling the DPCS (SDPC), the second set by adding extra charge points 1.0 Å above and below the C atoms and constructing the quadrupole moment by shifting the appropriate amount of charge from the C atoms to the extra charge points (EDPC). For the molecular polarizability three representations were studied as well. The first is Thole's standard model (P): atomic polarizabilities on the nuclei only. These yield a molecular polarizability that is over 10% below the experimental value (see Table II). Interestingly, the shortcoming of the polarizability in Thole's model is almost entirely due to the falling short of the out-of-plane component, which indicates that benzene is a special molecule and gives the same problems to Thole's model as for ab initio calculation of the polarizability. The failure of Thole's model can be repaired by scaling the polarizabilities (SP) or by adding extra polarizabilities above and below the plane (EP). For the latter we chose the same points as for the EDPCs. Parameters are given in Appendices 2 and 3. The computed binding energies with their interaction components are collected in Table III.

The results presented in Table III deserve close inspection because they give insight into some of the particulars of the DRF force field. Consider the electrostatic interaction. First note the error in the analysis of Hobza et al. [54], who report an attractive quadrupole–quadrupole interaction in the parallel-displaced dimer. Using the quadrupole tensors and interaction expression given by Buckingham [68], displacing a parallel benzene can indeed give electrostatic attraction, but the displacement should be quite a bit more than the 1.6 Å of the present minimum-energy conformation in which the electrostatic interaction is definitely repulsive. The electrostatic interaction is reproduced qualitatively by the standard DPCs, but because they recover only 60% of the overall quadrupole moment they yield electrostatic interaction energies that are smaller than they should be. The scaled DPCs do not quite reproduce the

TABLE II
Computed and experimental molecular properties of benzene.[a]

Model	$-\theta_{zz}$[b]	α_{xx}[c]	α_{zz}	$\langle\alpha\rangle$[d]
DZP[e]	7.10	71.8	27.1	56.9
DPC[f] from DZP	2.82			
DPC[f] from STO4-31G	4.66			
P[g]		74.2	36.3	61.5
SP[h]		84.6	40.2	69.8
EP[i]		76.4	53.4	69.8
Hobza et al. [54], DZ + 2P[j]	7.38	73.0	33.5	59.8
Hobza et al. [54], best[k]	7.08	79.2	44.5	67.7
Experimental[l]	7.4 ± .5			69.6

[a] All properties in atomic units.
[b] Buckingham [68] quadrupole. Note that $\theta_{xx} = \theta_{yy} = -1/2\theta_{zz}$ because of the molecular symmetry.
[c] $\alpha_{yy} = \alpha_{xx}$.
[d] Isotropic molecular polarizability.
[e] Expectation values from DZP-level HF for quadrupole and coupled HF for polarizability.
[f] DPCs (Ref. [13]) at the nuclei from HF wave function.
[g] Standard Thole model polarizabilities at the nuclei, exponential damping function (Ref. [14]).
[h] Scaled polarizabilities at the nuclei (see Appendix 3).
[i] Added polarizabilities 1 Å above and below the molecular plane (see Appendix 3).
[j] Taken from Hobza et al. [54]. Basis set used for calculation of binding energy.
[k] Hobza's best values, basis set includes two polarization functions on C and H, extra valence functions on C and H, and *f* functions on C.
[l] Refs. [66] and [67].

quadrupole–quadrupole interaction either, but this is not to be expected due to local effects and the operation of the damping function. This is better seen from the EDPCs, which are supposed to model the electronic clouds above and below the molecular plane by extra charge points. With these charges the electrostatic attraction and repulsion diminish with respect to the scaled DPCs. The spreading of the charge from the C atoms causes the major contributions to be dipole–dipole rather than charge–charge interactions, leaving the electrostatic interactions less pronounced. In addition to

TABLE III
Computed total and component binding energies of the benzene dimer.[a]

	Perpendicular (III)			Parallel-displaced (I)		
Model / Orientation	$\Delta U_{els}t$[b]	$\Delta U_{dis}p$[c]	ΔU_{tot}^{d}	$\Delta U_{els}t$[b]	$\Delta U_{dis}p$[c]	ΔU_{tot}^{d}
DPC-P	−2.0	−11.7	−7.8	+3.3	−17.3	−9.0
SDPC-P	−4.9	−11.7	−10.9	+8.0	−17.3	−5.1
EDPC-P	−3.7	−11.7	−9.9	+7.6	−17.3	−6.6
SDPC-SP	−4.9	−13.6	−12.8	+8.0	−20.5	−8.4
EDPC-EP	−3.7	−24.6	−15.8	+7.6	−48.2	−13.3
Hobza et al.[e]	−5.7	−3.4	−8.8	−6.2	−16.1	−9.5
QQ-London[f]	−5.7	−4.8	+11.3	−22.9		

[a] All energies in kJ / mol. The head-on perpendicular (R = 5.0 Å) and parallel-displaced (R_1 = 3.5 Å; R_2 = 1.6 Å) geometries are structures a and e taken from Hobza et al. [54].
[b] Electrostatic interaction energy.
[c] Dispersion contribution to interaction energy by Eq. (7) with distributed polarizabilities.
[d] Total binding energy.
[e] Hobza's analysis [54], made in terms of computed overall quadrupole moments and polarizabilities.
[f] Overall quadrupole-quadrupole interaction and London dispersion interaction from experimental polarizability and ionization energy.

the local effects, the damping function further reduces the interactions as it compensates for overlap effects.

The distributed polarizability representation strongly affects the dispersion energy for the perpendicular geometry, giving larger interactions than obtained from the London formula with isotropic molecular polarizabilities [69]. For the parallel-displaced geometry the DRF dispersion interactions are smaller, except for the EP representation which seems to overestimate the interaction, perhaps because the extra polarizabilities are too far from the molecular plane. The anisotropy of the distributed representation is essential for a balanced description of the correlation interaction, though. The ratio between the DRF dispersion energies for parallel-displaced and perpendicular geometries (1.5–2) is much closer to that from the ΔE^{MP2} values given by Hobza et al. [54] (2.3) than that from the London dispersion energies (4.8). With anisotropic molecular polarizabilities the ratio is about 2.6, emphasizing the inadequacy of the isotropic polarizability representation. The anisotropy of the benzene polarizability tensor is quite large, and the observation that the dispersion interaction is less orientation dependent than the electrostatic interaction [52, 54] is not valid for the benzene dimer.

The question of the relative stabilities of perpendicular and parallel-displaced geometries is unresolved by the DRF force field. Only the standard (DPC-P) DRF force field agrees with the best ab initio results available in giving preference to the parallel-displaced geometry. Any improvement of the description of molecular properties results in the perpendicular geometry being the more stable, however. We conjecture this corroborates better with experiments, noting that Hobza's best results are obtained with a basis set that underestimates the out-of-plane molecular polarizability, thereby putting the perpendicular geometry at a disadvantge with respect to the parallel-displaced one. As for the binding energy of the benzene dimer, a value of 10–12 kJ/mol seems to be the limit, which is somewhat larger than the experimental value of 7 ± 1 kJ/mol. Correction for zero-point energy lifts the experimental value to 9 ± 1 kJ/mol, however [57]. As a final check on the DRF force field binding energy and structure a potential energy surface (PES) scan was performed with the DPC-P and SDPC-SP parameter sets. The results are shown in Figure 8.

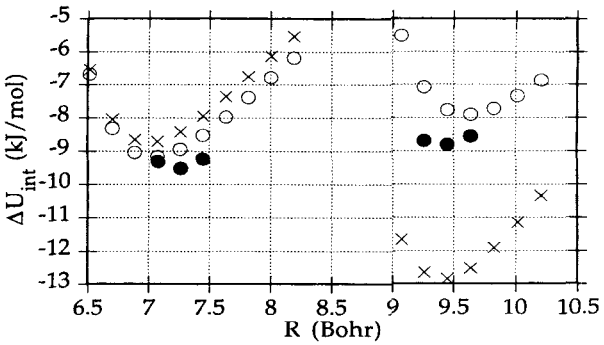

FIGURE 8. Benzene dimer interaction energy as a function of intermolecular distance. Left: parallel-displaced orientation; right: perpendicular orientation. (○) DPC-P parameters; (×) SDPC-SP parameters; (●) Hobza et al. [54].

The conclusions that may be drawn from the minimum-energy search and PES scan presented in Figure 8 are that the standard parametrization corresponds to the present ab initio results, whereas the extended parametrization points to possible improvements, corroborating with experimental results on structure, suggesting too small a value of the experimental binding energy.

DIMERS OF BENZENE DERIVATIVES

The dimers of toluene, *o*-xylene, and fluorobenzene, along with some mixed dimers were investigated by the standard DRF force field. Controlled PES scans along the intermolecular vector (R_1) were performed starting at perpendicular and parallel(-displaced) orientations. Parameters may be found in Appendix 2. The results of these calculations have been collected in Table IV.

The preferred orientation of the aromatic rings is parallel in all minimum-energy structures. This preference for parallel structures may be explained by the dominance of the dispersion contribution to the binding energy. A parallel orientation of the aromatic rings allows a much closer contact than a perpendicular arrangement, resulting in a larger dispersion interaction. The unfavorable electrostatic quadrupole–quadrupole interaction is a price worth paying. In the substituted benzenes some of the electrostatic repulsion between the quadrupoles may be made good by favorable dipole–dipole interactions. This explains the preference for antiparallel arrangements. The model calculations seem to contradict experimental findings in proteins that phenyl rings are often in some perpen-

dicular arrangement [53]. For all complexes except the *o*-xylene dimer we found perpendicular arrangements, mostly side-on to benefit from dipole–dipole attraction, that were within 5 kJ/mol of the (anti-)parallel minimum-energy structure. Improved description of the out-of-plane component of the polarizability is expected to bring these structures down in energy, like it did for the benzene dimer, and thus there seems to be no strong intrinsic dislike for perpendicular arrangements between substituted arenes.

The simple standard DRF force field yields binding energies for the molecular complexes of benzene derivatives that agree very well with experimental values. Only the benzene dimer itself is calculated to be more stable than what is found experimentally. In view of the underestimation of the polarizability in the DRF force field for benzene (Table II), we suggest that the experimental binding energy of benzene is too small. We cannot subscribe to the analysis of the factors determining th structure of arene complexes given by Hobza et al. [54] and by Hunter and Saunders [52], viz. that the electrostatic interaction determines the structure and the dispersion the binding energy. This conclusion was based on a faulty analysis of the quadrupole—quadrupole interaction. The dispersion interaction constitutes the main contribution to the binding energy. To maximize this interaction, the monomers will try to be as close to each other as possible. Acting against perpendicular arrangements are repulsive interactions due to the Pauli principle, much stronger than the electrostatic repulsion betwen quadrupoles in the parallel–displaced conformations. The precise minimum in the latter is, however, influenced by electrostatic interactions as a balance is struck between attraction and repulsion.

The Monte Carlo minimum-energy search does not yield surprising low-energy structures. The difference with the manual-search structures are only slight tilts of the aromatic rings. The benzene dimer exhibits a more pronounced tilt (24° between the principal moments of inertia). The observed predominance of perpendicular orientations must be explained by the thermal population of such structures. In this respect, the 5-kJ/mol difference we find between parallel and perpendicular structures must be regarded as an upper bound. We have demonstrated that improvement of the out-of-plane component of the polarizability tensor stabilizes perpendicular arrangements more

TABLE IV
Minimum energies[a] and corresponding structures[b] of molecular complexes between benzene derivatives.

Complex[c]	ΔU^{d}_{min}	ΔU_{elst}	ΔU_{disp}	Structure	U^{e}_{MC}	Lit.[f]
B–B	−9.0	+3.3	−17.3	Parallel-displaced (I); $R_1 = 6.4$; $R_2 = 2.9$ bohr	−9.8	-7 ± 1; *−9.6*
B–T	−11.9	−0.2	−18.6	Parallel-displaced (I); $R_1 = 6.1$; $R_2 = 5.2$ bohr	−14.0	-13 ± 2
T–T	−14.3	+2.8	−26.8	Anti-parallel-displaced (II); $R_1 = 6.7$; $R_2 = 0.4$ bohr	−15.0	-15 ± 2
T–X	−16.8	+2.1	−32.1	Anti-parallel-displaced (II); $R_1 = 6.6$; $R_2 = -0.3$ bohr	−17.5	-17 ± 3
X–X	−19.9	+0.6	−35.2	Anti-parallel-displaced (II); $R_1 = 6.7$; $R_2 = 0.3$ bohr	−20.3	-21 ± 3
F–F	−15.2	−1.8	−24.8	Anti-parallel-displaced (II); $R_1 = 6.4$; $R_2 = 1.0$ bohr	−15.3	

[a] All energies in kJ / mol. the parameter sets used were the standard DPCs and Thole's polarizabilities with the exponential demping function.
[b] For general features of the structures see Figure 7.
[c] Abbreviations used: B: benzene (X = Y = H); T: tolune (X = CH_3, Y = H); X: *o*-xylene (X = Y = CH_3); F: fluorobenzene (X = F, Y = H).
[d] Binding energy at minimum-energy conformation in controlled PES scan.
[e] Binding energy at minimum-energy conformation in a Monte Carlo sampling run at 100 K, starting from controlled PES-scan minimum.
[f] Literature experimental (Ref. 58) and computed binding energies. Italicized numbers are computational results. B-B from Hobza et al.

than parallel ones for the benzene dimer. It is to be expected this will be the same for the other complexes studied here, although toluene and *o*-xylene will need less reparation of the polarizability than benzene because they have out-of-plane centers that carry polarizabilities.

ACETONITRILE AND TETRACHLOROMETHANE DIMERS

To further investigate the generality of the proposed scheme to obtain force-field parameters, a comparison of calculated and experimental binding energies and equilibrium distances of acetonitrile (MeCN) and tetrachloromethane (CCl_4) dimers is reported in Table V. Force-field parameters are given in Appendices 1 and 2.

Although the computed binding energy of the MeCN dimer is not as large as fits to experimental data give [70], it does compare very well to Jorgensens liquid-phase interaction value of 16 kJ/mol [71]. Jorgensens model reproduced the heat of vaporization very well. The experimental uncertainty in the CCl_4 data is quite large, but the model interaction presented here compares well to those data. Note that CCl_4 was not part of the learning set from which atomic polarizabilities were fitted to molecular polarizabilities [14]. For the CCl_4 dimer a separate comparison is made for the repulsive part of the potential to test the CHARMM repulsion term. The classical CHARMM repulsion is compared to the orthogonalization energy in a DZP basis. The CHARMM repulsion is a little too hard at the DRF equilibrium distance, so the present binding energy and equilibrium distance may be considered as upper limits. This parametrization of MeCN and CCl_4 has been successfully employed in the calculation of the $\pi^* \leftarrow n$ solvatochromic shift of acetone in our combined quantum-mechanical–classical condensed-phase model [72].

Solvation Energy and Interactions in the Condensed Phase

The results for molecular dimers have been encouraging, and we are now in a position to study the behavior of our model in condensed-phase systems. Of special importance are the reliable computation of thermodynamic properties, such as the energy of solvation, and the correct representation of solvent electric potentials and fields at chromophores. Studies into these properties have been published already [2, 5, 6, 8, 72–74]. Here, we wish to review briefly the aqueous solution. Dielectric continuum models have been very popular in describing solvent effects in aqueous solution [75–95] but provide little detail of the molecular environment, because specific interactions are neglected. This shortcoming leads to a failure of consistency in application of the dielectric model, which is illustrated in Table VI, in which we have collected the solvation free energies of a number of different solutes.

The solutes are described quantum chemically. Two definitions of the solute–solvent boundary have been used [99]: a near boundary, with scaled van der Waals radii on the solute atoms, and a distant boundary, with atomic radii that are the sum of the van der Waals and solvent water radii. The electrostatic and dispersion components to the solvation free energy are very sensitive to the position of the boundary. With a consistent choice of solute–solvent boundary distance, one may reproduce the solvation free energy for some solutes, but not all. For near boundaries, the dispersion interaction is absurdly large due to "charge leak-

TABLE V
Calculated and experimental binding energies and equilibrium distances for MeCN and CCl_4 dimers.

	$-\Delta U_{int}$ (kJ/mol)			R_{eq} (Bohr)		
Species	DRF[a]	Comp.[b]	exp.[c]	DRF[a]	Comp.[b]	exp.[c]
MeCN	15.5	16[71]	21.8[70]	6.64		6.52
CCl_4	3.1		3.8 ± 1.1[114]	10.9		10.5 ± 0.5

[a] Classical DRF force field.
[b] Ab initio or other force field.
[c] Experimental results.

TABLE VI
Solvation free energies[a] of various solutes in water, calculated in the dielectric continuum solvent model.[b]

Solute	$\Delta G_{ex}p$[e]	$\Delta G_{ca}v$[f]	$\Delta G_{int}g$	Van der Waals[c]		vdW + solvent[d]	
				$\Delta G_{elst}h$	$\Delta G_{dis}p$[i]	$\Delta G_{elst}h$	$\Delta G_{dis}p$[i]
MeCN[j]	−16.3	+8.5	−24.8	−44	−151	−6	−18
Me_2CO[k]	−16.1	+7.3	−23.4	−29	−195	−4	−30
H_2O[j]	−26.5	+13.8	−40.3	−22	−72	−3	−10
MeOH[j]	−21.4	+9.6	−31.0	−13	−140	−2	−16
C_6H_5Me[k]	−3.7	+6.3	−10.0	−73	−386	−4	−53
C_6H_6[k]	−3.6	+6.7	−10.3	−45	−258	−8	−49
CCl_4[j]	+0.4	+6.5	−6.1	−1	−225	0	−41

[a] All energies in kJ / mol.
[b] The solute–solvent boundary Connolly's solvent-accessible surface [99] with probe radius of 3.64 bohrs, generated by the program MSCON, and consists of approximately 300 boundary elements. Poisson's equations are solved in the constant-element version of the method by Juffer et al. [96].
[c] Atomic radii to define the size of the cavity are the van der Waals radii scaled by 1.2. The solute is represented by its *vacuum* density.
[d] Atomic radii to define the size of the cavity are the van der Waals radii plus the water radius (3.64 bohrs). The solute density is coupled *self-consistently* to the reaction potential.
[e] Experimental solvation free energy [97].
[f] Cavitation free energy, calculated with Pierotti's method, [98] with solute and solvent diameters from pure substance density [67].
[g] Interaction free energy, $\Delta G_{exp} - \Delta G_{cav}$, to be reproduced by electrostatic and dispersion interactions in the dielectric continuum model.
[h] Electrostatic component to solvation free energy; $\varepsilon_0 = 78.5$.
[i] Dispersion component to electrostatic free energy, computed analogously to Eq. (8), with U_A and U_S the experimental ionization energies [67] of solute and solvent, respectively; $\varepsilon_\infty = 1.78$.
[j] DZP basis set.
[k] STO4-31G basis set.

age" of the solute into the continuum region [8], which also causes failure of the density to converge if the reaction potential is coupled back to the solute.

Although computationally more costly than dielectric continuum models, explicit solvent models [6, 28, 33, 100–107] are worth studying in their own right since they provide so much more information on and insight into the factors that play a role in the solvation process. The main advantage is that explicit solvent models are expected to be more generally valid because their parametrization is at a deeper level than that of the dielectric models.

A number of the solutes studied with the dielectric continuum solvent model were immersed in a number of our explicit, polarizable water molecules. The explicit molecules were embedded in a dielectric with a distant Connolly surface boundary. A Monte Carlo sampling [108] of the orientational and translational degrees of freedom was performed [9], with a cut-off radius to prevent the solvent molecules entering the continuum [6]. The energy of solvation was calculated by subtracting the average total energy of the solvent molecules alone from that of the solute plus solvent system:

$$\Delta U_{solv} = \langle U_{int} \rangle_s + \langle U_N \rangle_s - \langle U_N \rangle_0 \qquad (11)$$

in which $\langle\ \rangle_s$ denotes an average over the configurations of the solvent molecules in the presence of the solute, and $\langle\ \rangle_c$ in the absence of the solute, but in the same volume. U_N is the total energy of the N explicitly treated solvent molecules, U_{int} the interaction energy between the solute and N solvent molecules. The interaction components have been analyzed. The results are shown in Table VII.

The results of the explicit solvent model deserve some discussion. The solvation energies of water, acetone, and acetonitrile are seen to be in quite good agreement with experiment [97]. Only the solvation energy of methanol in water is some way off the experimental value. This may be due to insufficient sampling, in combination with equilibration of the system before collecting the data. In the runs we have performed the number of sampling steps is rather small (about 2000 trial moves

per solvent molecule). As far as the *interaction* energy between solute and solvent is concerned, proper equilibration was not very important. This was not so for the solvation energy, which is a difference between two total energies. The reliability of the results will improve if the sampling is extended. It would be well worthwhile to study the DRF force field with more sophisticated and direct thermodynamic ways to obtain the solvation energy [100]. Nevertheless, the present results show the general validity of the explicit water model. Rullmann has applied this model to calculate protonation energies of amines in water [6]. His simulations were more extensive, both in number of MC steps and in number of solvent molecules considered.

The interaction energy of water in water was investigated in more detail. The aims of this study are the comparison of the quantum-chemical description of the solute to the classical one, and the investigation of the extent to which solvent molecules need to be described explicitly. First, the water pentamer was studied. The central water is surrounded by four water molecules. The surrounding molecules are placed at optimal distances and angles, taken from the water dimer. This configuration is studied both with and without a surrounding dielectric continuum to estimate the bulk contribution. Next, a Monte Carlo sampling of the orientational degrees of freedom is performed, keeping the centers of gravity at their original positions. Finally, translational freedom of the surrounding molecules is allowed as well. The results of these calculations are presented in Table VIII.

The agreement between quantum-mechanical and classical descriptions has been pointed out before [8]. There are some comments to be made on this, however. Although the agreement between mixed and fully classical descriptions is good for the total interaction energy between solute and solvent, this may not be so for the individual components. This is especially true for the dispersion interaction, which is invariably larger for the classical solute than it is for the quantum-mechanical one. This is explained by the fact that the classical solute model reproduces the experimental polarizability of water very well, whereas the DZP basis falls well short, which has been noted in the discussion of the water properties (Table I). On the other hand, the electrostatic interaction is seen to be larger in the quantum-mechanical solute case. This is due to the use of the basis set, which extends more into the solvent than the point charges do in the classical treatment.

The main solute–solvent interaction is seen to be captured by including only the first solvation shell. For water in water building the first solvation shell is easy, as the structure of the water pentamer is quite well known. For other solutes and solvents such a procedure would be more difficult. Including only the first solvation shell in the way it is done here can be deceptive, though. All solute–solvent interactions are optimal. This may be true at 0 K and in the gas phase, but it s not a realistic picture of the condensed phase at room temperature. Allowing rotation of the four first-shell molecules already raises the energy, and allowing translation reenforces this trend. As more solvent molecules are added, saturation will occur.

TABLE VII
Solvation energies[a] of various solutes in water, calculated by the explicit solvent model.[b]

Solute	ΔU_{elst}	ΔU_{disp}	ΔU_{rep}	ΔU_{int}	ΔU_{solv}	ΔU_{exp}
H_2O[c]	−66	−39	+40	−65 ± 8	−35	−41
CH_3COCH_3[c]	−52	−76	+53	−75 ± 12	−33	−40
CH_3CN[d]	−53	−56	+48	−61 ± 11	−32	−32
CH_3OH[d]	−40	−54	+40	−54 ± 8	−61	−44

[a] All energies in kJ / mol.
[b] ΔU_{solv} is calculated by Eq. (11). The solvent translational and rotational degrees of freedom are sampled in 50,000 Monte Carlo steps.
[c] 236 surrounding water molecules.
[d] 25 surrounding water molecules.

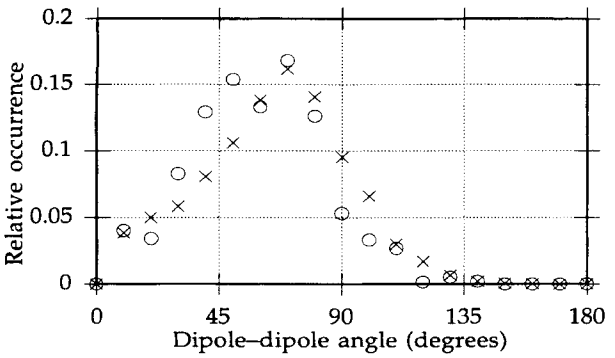

FIGURE 9. Comparison of the relative dipole–dipole angle occurrence for the water pentamer in various descriptions, with fixed center of mass distance (for details of the simulation, see text). (○) mixed description; (×) fully classical description.

As far as the interaction between solute and solute is concerned we suggest that the 26 water molecules are adequate. For accurate calculations on thermodynamic processes, such as solvation energy, boundary effects may necessitate more explicitly described solvent molecules before terminating in a continuum [5, 6, 109]. Nevertheless, it is clear that addition of a discrete first solvent shell is an essential improvement on the dielectric-only model.

The slight discrepancies between the individual interaction energy contributions for a quantum-chemical and classical central water molecule might raise questions on the structural behavior of the surrounding molecules. The orientation of the surrounding water molecules with respect to the central water has been investigated for the water–pentamer system in the gas phase (entries 1 and 3 in Table VIII) and is shown in Figure 9. It is seen that the maxima of the dipole–dipole angle distributions coincide, but that the shape of the distribution differs somewhat between the mixed and fully classical descriptions. In particular, in the fully classical model the distribution is somewhat shifted to larger angles. The difference is not too drastic, though, and the irregularities in the mixed curve suggest that the sampling should be more extensive.

Conclusion

The DRF force field is shown to provide a simple, general scheme to parametrized atom-based interaction functions that closely follow the theoretical intermolecular interaction components: electrostatic, induction, dispersion, and repulsion. The advantage of such a scheme is that the description can easily and systematically be improved according to the required accuracy as more detailed information on the molecules become available, either from experiment or from accurate

TABLE VIII
Total interaction energy of a water molecule with surrounding water and analysis of the interaction contributions.[a] Comparison of the description of the solute charge distribution.

Solute / Solvent Model[b]	ΔU_{int}	ΔU_{elst}	ΔU_{disp}	ΔU_{rep}
DZP / 4 classical[c]	−60 ± 5 (−67)	−77 (−89)	−15 (−15)	+27 (+30)
DZP / 4 classical + diel.[d]	−66 ± 5 (−81)	−79 (−89)	−18 (−18)	+26 (+30)
Clas./ 4 classical[c]	−58 ± 5 (+76)	−74 (−81)	−26 (−27)	+28 (+30)
Clas./ 4 classical + diel.[d]	−70 ± 5 (−86)	−72 (−82)	−25 (−27)	+28 (+30)
DZP / 26 classical + diel.[e]	−69 ± 17 (−68)	−67 (−72)	−30 (−32)	+40 (+39)
Clas./ 26 classical + diel.[e]	−68 ± 8 (−72)	−66 (−69)	−39 (−41)	+40 (+39)

[a] All energies in kJ / mol. The values in parentheses reflect the reference, or start, geometry.
[b] DZP indicates the solute water being treated quantum mechanically in the DZP basis; classical indicates the solute water being treated classically, like the surrounding water molecules (parameters for the classical water [experimental molecular polarizability] may be found in Appendix 2); Diel. denotes the addition of a dielectric continuum term (the boundary is located at the solvent-accessible surface, traced out from spheres located at the water centers of gravity).
[c] 15,000 trial moves, rotation only.
[d] 15,000 trial moves, rotation and translation.
[e] 100,000 trial moves, rotation and translation.

quantum-chemical calculations. An important advantage of the DRF force field over other force fields such as CHARMM [24], AMBER [110, 111], and GROMOS [112, 113] is the clear separation of parameters, one set for each interaction component. In this way each component can be improved independently from the others. Especially the separation of electrostatic and induction interactions through explicit modeling of response properties avoids parametrization in which the immediate surrounding of an atom is incorporated in nontransparent ways. For example, there is no need to distinguish between alcoholic, aldehydic, and carboxylic oxygens for nonbounded interactions in the DRF force field.

Problems only arise at shorter distances where modeling of the consequences of the antisymmetry requirement on the total wave function becomes impossible. At intermediate distances the *ad hoc* repulsion potentials may be used to fine-tune the interaction potential depth and location of the minimum. There is a need for a more general repulsive potential in the spirit of the present approach.

Modeling of the first solvation shell(s) by molecular electrostatic (and response) models does not suffer from the inconsistencies of the dielectric-only model. Such an approach is more costly, however, and there may be problems regarding the number of explicit molecules to be included before terminating the explicitly described region by a dielectric. Boundary effects should be minimized. The property of interest will decide to some extent the length to which one should go. If macroscopic thermodynamic properties are wanted, such as solvation energies, one should not be easily satisfied. If, however, the potentials and fields at a microscopic region due to the surrounding medium are of interest, explicit description of the first two shells will generally suffice.

Appendix 1

GENERAL DRF FORCE FIELD PARAMETERS

The parameters given in Table A1 are used throughout this paper, unless noted otherwise. For the repulsion the radii of set I are used throughout, except for the benzene-derived dimers, for which set II is used. Further deviation from the parameters given is only for the polarizabilities of H and O in water when fitted to the DZP polarizability (Table I; Figs. 2–4); and for H and C in the benzene SDPC, EDPC, SP, and EP parmeterizations, which are given in Appendix 3.

TABLE A1
Atomic polarizabilities and radii for use in computation of induction, dispersion, and repulsion energies.

Damping[a]	Exponential	Linear	Repulsion	
Width parameter[a]	2.089	1.662	I	II
Atom	polarizability[b]	polarizability[b]	Radius[c]	Radius[c]
H	2.881	3.469	2.516	2.267
C	8.672	9.482	3.518	3.213
N	6.526	7.457	3.247	2.929
O	5.304	5.871	2.989	2.872
F	3.200	3.577		2.778
Cl	17.61	17.61	4.324	3.307

[a] Thole's damping functions 1 and 4, respectively, see ref. [14].
[b] In Bohr^3.
[c] In Bohr.

APPENDIX 2

DRF FORCE-FIELD PARAMETERS AND COMPUTED MOLECULAR PROPERTIES FOR MOLECULES USED IN THIS STUDY

TABLE A2

Atomic Cartesian coordinates, partial charges, computed overall dipole and quadrupole moments, and computed polarizability.

Molecule	X^a	Y^a	Z^a	q^b	μ, θ^c	α^d
Water[e]					0.787	9.8
O	0.0	0.0	0.0	−0.796	−0.06	9.4
H (O_1)	1.1031	1.4325	0.0	+0.398	1.26	12.3
H (O_2)	1.1031	−1.4325	0.0	+0.398	−1.19	7.6
Benzene[f]					0.0	61.5
C (1)	0.0	−2.63995	0.0	−0.1035	2.33	74.2
C (2)	−2.28626	−1.31997	0.0	−0.1035	2.33	74.2
C (3)	−2.28626	1.31997	0.0	−0.1035	−4.66	36.3
C (4)	0.0	2.63995	0.0	−0.1035		
C (5)	2.28626	1.31997	0.0	−0.1035		
C (6)	2.28626	−1.31997	0.0	−0.1035		
H (C_1)	0.0	−4.68841	0.0	0.1035		
H (C_2)	−4.06028	−2.34421	0.0	0.1035		
H (C_3)	−4.06028	2.34421	0.0	0.1035		
H (C_4)	0.0	4.68841	0.0	0.1035		
H (C_5)	4.06028	2.34421	0.0	0.1035		
H (C_6)	4.06028	−2.34421	0.0	0.1035		
Toluene[f]					0.11	74.4
C (1)	0.0	−2.63995	0.0	−0.1150	2.02	83.6
C (2)	−2.28626	−1.31997	0.0	−0.1097	2.00	92.0
C (3)	−2.28626	1.31997	0.0	−0.1533	−4.02	47.5
C (4)	0.0	2.63995	0.0	−0.1868		
C (5)	2.28626	1.31997	0.0	−0.1556		
C (6)	2.28626	−1.31997	0.0	−0.1043		
H (C_1)	0.0	−4.68841	0.0	0.0991		
H (C_2)	−4.06028	−2.34421	0.0	0.1016		
H (C_3)	−4.06028	2.34421	0.0	0.1048		
C (7)	0.0	5.55013	0.0	0.3860		
H (C_5)	4.06028	2.34421	0.0	0.1037		
H (C_6)	4.06028	−2.34421	0.0	0.1015		
H (C_{71})	1.94202	6.23668	0.0	0.1028		
H (C_{72})	−0.97101	6.23668	1.68183	0.1118		
H (C_{73})	−0.97101	6.23668	−1.68183	0.1118		
o-Xylene[f]					0.20	86.8
C (1)	0.0	−2.63995	0.0	−0.1159	1.65	100
C (2)	−2.28626	−1.31997	0.0	−0.1205	1.73	103
C (3)	−2.28626	1.31997	0.0	−0.1563	−3.38	57.8
C (4)	0.0	2.63995	0.0	0.1331		
C (5)	2.28626	1.31997	0.0	0.1322		
C (6)	2.28626	−1.31997	0.0	−0.1566		
H (C_1)	0.0	−4.68841	0.0	0.0973		
H (C_2)	−4.06028	−2.34421	0.0	0.0973		
H (C_3)	−4.06028	2.34421	0.0	0.1033		
C (7)	0.0	5.55013	0.0	−0.3815		
C (8)	4.80655	2.77507	0.0	−0.3849		
H (C_6)	4.06028	−2.34421	0.0	0.1026		
H (C_{71})	1.94202	6.23668	0.0	0.1133		
H (C_{72})	−0.97101	6.23668	1.68183	0.1064		
H (C_{73})	−0.97101	6.23668	−1.68183	0.1064		
H (C_{81})	6.37213	1.43651	0.0	0.1036		
H (C_{82})	4.91511	3.96013	1.68183	0.1101		
H (C_{83})	4.91511	3.96013	−1.68183	0.1101		

(Continued)

TABLE A2
Continued

Fluorobenzene[f]					0.80	62.1
C (1)	0.0	−2.63995	0.0	−0.1243		74.6
C (2)	−2.28626	−1.31997	0.0	−0.1112		74.8
C (3)	−2.28626	1.31997	0.0	−0.2134		36.8
C (4)	0.0	2.63995	0.0	0.5658		
C (5)	2.28626	1.31997	0.0	−0.2134		
C (6)	2.28626	−1.31997	0.0	−0.1112		
H (C_1)	0.0	−4.68841	0.0	0.1034		
H (C_2)	−4.06028	−2.34421	0.0	0.1161		
H (C_3)	−4.06028	2.34421	0.0	0.1213		
F (C_4)	0.0	6.41657	0.0	−0.3705		
H (C_5)	4.06028	2.34421	0.0	0.1213		
H (C_6)	4.06028	−2.34421	0.0	0.1161		
Acetonitrile[e]					1.67	29.3
C (CN)	0.0	0.0	0.0	+0.5050	−1.52	38.3
N	−2.20	0.0	0.0	−0.5090	0.76	24.7
C (Me)	2.81	0.0	0.0	−0.8360	0.76	24.7
H (C_{21})	3.45	−1.81	0.0	+0.2800		
H (C_{22})	3.45	0.90	1.57038	+0.2800		
H (C_{23})	3.45	0.90	−1.57038	+0.2800		
Acetone[f, g]					1.50	42.4
C (CO)	0.46479	0.95640	−0.00905	+0.61375	0.64	46.0
O	1.68667	2.89733	0.00450	−0.52335	−1.70	45.2
C (Me 1)	−2.37519	0.98510	−0.00004	−0.37730	1.06	36.0
H (C_{11})	−3.09296	0.00491	1.64946	+0.11070		
H (C_{12})	−3.10363	0.01723	−1.65125	+0.11070		
H (C_{13})	−3.05158	2.90761	0.01028	+0.11070		
C (Me 2)	1.71788	−1.59275	−0.02687	−0.37730		
H (C_{21})	1.20654	−2.64285	1.65643	+0.11070		
H (C_{22})	1.09693	−2.68784	−1.64194	+0.11070		
H (C_{23})	3.74285	−1.37428	−0.09414	+0.11070		
Methanol[e, h]					0.76	22.5
C	−0.71167	−0.15571	0.27004	−0.0139	0.18	23.7
O	1.95454	−0.15571	0.27004	−0.6021	−0.63	21.3
H (OH)	2.49028	0.68843	−1.25289	0.4111	0.45	22.6
H (C_{21})	−1.46813	1.81716	0.27004	+0.0545		
H (C_{22})	−1.47096	−1.20376	−1.40218	+0.0545		
H (C_{23})	−1.26498	−1.14933	2.05319	+0.0959		
Tetrachloromethane[e]					0.0	73.5
C	−0.058959	0.0	0.043464	−0.1944	0.0	73.5
Cl (1)	3.266958	0.0	0.043464	0.0486	0.0	73.5
Cl (2)	−1.167662	−3.135811	0.043464	0.0486	0.0	73.5
Cl (3)	−1.167662	1.567906	2.759000	0.0486		
Cl (4)	−1.167662	1.567906	−2.672072	0.0486		

[a] Cartesian coordinate in Bohr.
[b] Partial charge from HF wave function DPC analysis in atomic charge-units.
[c] Overall dipole moment in a.u. (1 a.u. = 2.54 D = 8.478 10^{-30} cm), and *xx*, *yy*, and *zz* components of the Buckingham quadrupole-moment tensor in a.u. (1 a.u. = 4.487 10^{-40} cm^2).
[d] Isotropic polarizability, and *xx*, *yy*, and *zz* components of molecular polarizability tensor in $Bohr^3$.
[e] DZP basis.
[f] STO4-31G basis set.
[g] STO4-31G-optimized geometry.
[h] AM1-optimized geometry (CaChe system).

Appendix 3

SPECIAL BENZENE MODEL PARAMETERS

Scaled models: SDPC and SP

The atomic charges and polarizabilities are scaled to yield the experimental quadrupole moment and isotropic molecular polarizability. The charges are $-0.1626e$ and $+0.1626e$; the polarizabilities are 10.0 and 3.4 for C and H, respectively, with Thole's standard exponential damping model.

Extra-center models: EDPC and EP

Extra charge and polarizability points are added 1.8897 bohrs (1.0 Å) above and below the C atoms in the z direction. The extra points are given a charge of $-0.07e$, a polarizability of 1.3 bohrs^3, and a radius of 1.3 bohrs. Each C charge is corrected to $+0.0365e$ (from $-0.1035e$) to neutralize the charge shift to the extra points. The H charges are unaltered.

ACKNOWLEDGMENTS

This work was sponsored by the Netherlands Foundation for Chemical Research (SON) and the National Computing Facilities Foundation (NCF) for the use of supercomputer facilities, with financial support from the Netherlands Organisation for the Advancement of Research (NWO).

References

1. B. T. Thole and P. Th. van Duijnen, Theor. Chim. Acta **55**, 307 (1980).
2. J. P. Dijkman and P. Th. van Duijnen, Int. J. Quantum Chem., Quantum Biol. Symp. **18**, 49 (1991).
3. B. T. Thole and P. Th. van Duijnen, Chem. Phys. **71**, 211 (1982).
4. P. Th. van Duijnen, M. Dupuis, and B. T. Thole, IBM DSD KGN-38, May 18, 1986.
5. J. A. C. Rullmann and P. Th. van Duijnen, Mol. Phys. **61**, 293 (1988).
6. J. A. C. Rullmann and P. Th. van Duijnen, Mol. Phys. **63**, 451 (1988).
7. P. Th. van Duijnen, A. H. Juffer, and J. P. Dijkman, J. Mol. Struct. (Theochem) **260**, 195 (1992).
8. A. H. de Vries, P. Th. van Duijnen, and A. H. Juffer, Int. J. Quantum Chem., Quantum Chem. Symp. **27**, 451 (1993).
9. A. H. de Vries, P. Th. van Duijnen, A. H. Juffer, J. A. C. Rullmann, J. P. Dijkman, H. Merenga, and B. T. Thole, J. Comp. Chem. **16**, 37 (1995).
10. P. Claverie, in *Intermolecular Interactions: From Diatomics to Biopolymers*, B. Pullman, Ed. (Wiley, Chichester, 1978), Chap. 69.
11. A. van der Avoird, P. E. S. Wormer, F. Mulder, and R. M. Berns, in *Topics in Current Chemistry*, F. L. Boschke, Ed. (Springer Verlag, Berlin, 1980), Chap. 1.
12. R. McWeeny, *Methods of Molecular Quantum Mechanics* (Academic Press, London, 1989), Chap. 14.
13. B. T. Thole and P. Th. van Duijnen, Theor. Chim. Acta **63**, 209 (1983).
14. B. T. Thole, Chem. Phys. **59**, 341 (1981).
15. G. Chalasinski and M. M. Szszesniak, Chem. Rev. **94**, 1723 (1994).
16. S. F. Boys and F. Bernardi, Mol. Phys. **19**, 553 (1970).
17. F. B. van Duijneveldt, J. G. C. M. van Duijneveldt-van de Rijdt, and J. H. van Lenthe, Chem. Rev. **94**, 1873 (1994).
18. R. J. Vos, R. Hendriks, and F. B. van Duijneveldt, J. Comp. Chem. **11**, 1 (1990).
19. K. Ohta, Y. Yoshioka, K. Morokuma, and K. Kitaura, Chem. Phys. Lett. **101**, 12 (1983).
20. V. Luaña and L. Pueyo, Phys. Rev. B **39**, 11093 (1989).
21. R. Colle and O. Salvetti, Theor. Chim. Acta **80**, 63 (1991).
22. L. Seijo and Z. Barandarian, J. Chem. Phys. **94**, 8158 (1991).
23. M. von Arnim and S. D. Peyerimhoff, Theor. Chim. Acta **87**, 41 (1993).
24. B. R. Brooks, R. E. Bruccoleri, B. D. Olafson, D. J. States, S. J. Swaminathan, and M. Karplus, J. Comp. Chem. **4**, 187 (1983).
25. J. G. Ángyán and G. Jansen, Chem. Phys. Lett. **175**, 313 (1990).
26. J. C. Slater and J. G. Kirkwood, Phys. Rev. **37**, 682 (1931).
27. E. Clementi and P. Habitz, J. Phys. Chem. **87**, 2815 (1983).
28. A. Wallqvist, P. Ahlström, and G. Karlström, J. Phys. Chem. **94**, 1649 (1990).
29. C. Millot and A. J. Stone, Mol. Phys. **77**, 439 (1992).
30. J. R. Reimers, J. O. Watts, and M. L. Klein, Chem. Phys. **64**, 95 (1982).
31. I. Ruff and D. J. Diestler, J. Chem. Phys. **93**, 2032 (1990).
32. H. J. C. Berendsen, J. P. M. Postma, W. F. van Gunsteren and J. Hermans, in *Intermolecular Forces; Proceedings of the 14th Jerusalem Symposium on Quantum Chemistry and Biochemistry*, B. Pullman, Ed. (Reidel, Dordrecht, 1981), Chap. 331.
33. W. L. Jorgensen, J. Chandraskhar, J. D. Madura, R. W. Impey, and M. L. Klein, J. Chem. Phys. **79**, 926 (1983).
34. H. J. C. Berendsen, J. R. Grigera, and T. P. Straatsma, J. Phys. Chem. **91**, 6269 (1987).
35. M. Sprik and M. L. Klein, J. Chem. Phys. **89**, 7556 (1988).
36. P. Cieplak, P. Kollman, and T. Lybrand, J. Chem. Phys. **92**, 6755 (1990).
37. G. Corongiu, Int. J. Quantum Chem. **42**, 1209 (1992).
38. B. Jeziorski and M. van Hemert, Mol. Phys. **31**, 713 (1976).
39. K. Szalewicz, S. J. Cole, W. Kolos, and R. J. Bartlett, J. Phys. Chem. **89**, 3662 (1988).

40. J. G. C. M. van Duijneveldt-van de Rijdt and F. B. van Duijneveldt, J. Chem. Phys. **97**, 5019 (1992).
41. S. Scheiner, Ann. Rev. Phys. Chem. **45**, 23 (1994).
42. T. H. Dunning Jr. and P. J. Hay, in *Methods of Electronic Structure Theory*, H. F. Schaefer III, Ed. (1977), Chap. 1.
43. L. A. Curtiss and M. Blander, Chem. Rev. **88**, 827 (1988).
44. M. C. van Hemert and C. E. Blom, Mol. Phys. **43**, 229 (1981).
45. J. Verhoeven and A. Dymanus, J. Chem. Phys. **52**, 3222 (1970).
46. G. H. F. Diercksen and A. J. Sadlej, J. Chem. Phys. **75**, 1253 (1981).
47. T. R. Dyke and J. S. Muenter, J. Chem. Phys. **59**, 3125 (1973).
48. C. E. Dykstra, S.-Y. Liu, and D. J. Malik, in *Advances in Chemical Physics*, I. Prigogine and S. A. Rice, Eds. (Wiley, New York, 1989), Chap. 37.
49. M. Urban and A. J. Sadlej, Theor. Chim. Acta **78**, 189 (1990).
50. W. Liptay, in *Excited States*, E. C. Lim, Ed. (Academic Press, New York, 1974), Chap. 129.
51. A. van der Avoird, P. E. S. Wormer, and R. Moszynski, Chem. Rev. **94**, 1931 (1994).
52. C. A. Hunter and J. K. M. Saunders, J. Am. Chem. Soc. **112**, 5525 (1990).
53. C. A. Hunter, J. Singh, and J. M. Thornton, J. Mol. Biol. **218**, 837 (1991).
54. P. Hobza, H. L. Selzle, and E. W. Schlag, J. Am. Chem. Soc. **116**, 3500 (1994).
55. B. R. Veenstra, H. T. Jonkman, and J. Kommandeur, J. Phys. Chem. **98**, 3538 (1994).
56. B. Ernstberger, H. Krause, A. Kiermeier, and H. J. Neusser, J. Chem. Phys. **92**, 5285 (1990).
57. H. Krause, B. Ernstberger, and H. J. Neusser, Chem. Phys. Lett. **184**, 411 (1991).
58. H. J. Neusser and H. Krause, Chem. Rev. **94**, 1829 (1994).
59. P. Hobza, H. L. Selzle, and E. W. Schlag, Chem. Rev. **94**, 1767 (1994).
60. G. Karlström, P. Linse, A. Wallqvist, and B. Jönsson, J. Am. Chem. Soc. **105**, 3777 (1983).
61. B. W. van de Waal, Chem. Phys. Lett. **123**, 69 (1986).
62. N. L. Allinger and J.-H. Lii, J. Comp. Chem. **8**, 1146 (1987).
63. W. L. Jorgensen and D. L. Severance, J. Am. Chem. Soc. **112**, 4768 (1990).
64. E. Arunan and H. S. Gutowsky, J. Chem. Phys. **98**, 4294 (1993).
65. V. A. Venturo and P. M. Felker, J. Chem. Phys. **99**, 748 (1993).
66. M. R. Battaglia, A. D. Buckingham, and J. H. Williams, Chem. Phys. Lett. **78**, 421 (1981).
67. *CRC Handbook of Chemistry and Physics* (CRC Press, Boca Raton, FL, 1983–1984).
68. A. D. Buckingham, in *Intermolecular Interactions: From Diatomics to Biopolymers*, B. Pullman, Ed. (Wiley, Chichester, 1978), Chap. 1.
69. F. London, Zeitschrift der Physik **63**, 245 (1930).
70. H. J. Böhm, I. R. McDonald, and P. A. Madden, Mol. Phys. **49**, 347 (1983).
71. W. L. Jorgensen and J. M. Briggs, Mol. Phys. **63**, 547 (1988).
72. A. H. de Vries and P. Th. van Duijnen, Int. J. Quantum Chem. **57**, 1067 (1995).
73. B. T. Thole and P. Th. van Duijnen, Biophys. Chem. **18**, 53 (1983).
74. J. A. C. Rullmann, M. N. Bellido, and P. Th. van Duijnen, J. Mol. Biol. **206**, 101 (1989).
75. S. Miertus, E. Scrocco, and J. Tomasi, Chem. Phys. **55**, 117 (1981).
76. K. V. Mikkelsen, H. Agren, H. J. Aa. Jensen, and T. Helgaker, J. Chem. Phys. **89**, 3086 (1988).
77. M. W. Wong, M. J. Frisch, and K. B. Wiberg, J. Am. Chem. Soc. **113**, 4776 (1991).
78. V. Dillet, D. Rinaldi, and J.-L. Rivail, Chem. Phys. Lett. **202**, 18 (1993).
79. V. Dillet, D. Rinaldi, and J.-L. Rivail, J. Phys. Chem. **98**, 5034 (1994).
80. K. V. Mikkelsen, P. Jørgensen, and H. J. Aa. Jensen, J. Chem. Phys. **100**, 6597 (1994).
81. B. Mennucci, M. Cossi, and J. Tomasi, J. Chem. Phys. **102**, 6837 (1995).
82. A. A. Rashin, M. A. Bukatin, J. Andzelm, and A. T. Hagler, Biophys. Chem. **51**, 375 (1994).
83. R. J. Hall, M. M. Davidson, N. A. Burton, and J. H. Hillier, J. Phys. Chem. **99**, 921 (1995).
84. A. Fortunelli and J. Tomasi, Chem. Phys. Lett. **231**, 34 (1995).
85. M. M. Karelson, T. Tamm, A. R. Katritzky, M. Szefran, and M. C. Zerner, Int. J. Quantum Chem. **37**, 1 (1990).
86. C. J. Cramer and D. G. Truhlar, J. Am. Chem. Soc. **113**, 8305 (1991).
87. C. J. Cramer and D. G. Truhlar, J. Comp. Chem. **13**, 1089 (1992).
88. M. Karelson, T. Tamm, and M. C. Zerner, J. Phys. Chem. **97**, 11901 (1993).
89. G. Rauhut, T. Clark, and T. Steinke, J. A. Chem. Soc. **115**, 9174 (1993).
90. M. K. Gilson, K. A. Sharp, and B. H. Honig, J. Comp. Chem. **9**, 327 (1987).
91. R. J. Zauhar and R. S. Morgan, J. Comp. Chem. **9**, 171 (1988).
92. H. Alper and R. M. Levy, J. Chem. Phys. **99**, 9847 (1993).
93. F. Schmidt, Mol. Sim. **13**, 347 (1994).
94. H. S. Shang and T. Head-Gordon, J. Am. Chem. Soc. **116**, 1528 (1994).
95. I. G. Tironi, R. Sperb, P. E. Smith, and W. F. van Gunsteren, J. Chem. Phys. **102**, 5451 (1995).
96. A. H. Juffer, E. F. F. Botta, B. A. M. van Keulen, A. van der Ploeg, and H. J. C. Berendsen, J. Comp. Phys. **97**, 144 (1991).
97. A. Ben-Naim and Y. Marcus, J. Chem. Phys. **81**, 2016 (1984).
98. R. A. Pierotti, Chem. Rev. **76**, 717 (1976).
99. M. L. Connolly, Science **221**, 709 (1983).
100. M. Mezei, Mol. Phys. 47, 1307 (1982).

101. C. Medina-Llanos, H. Ågren, K. V. Mikkelsen, and H. J. Aa Jensen, J. Chem. Phys. **90**, 6422 (1989).
102. V. V. Vasilyev, A. A. Bliznyuk, and A. A. Voityuk, Int. J. Quantum Chem. **44**, 897 (1992).
103. J. Gao and X. Xia, Science **258**, 631 (1992).
104. M. M. Karelson and M. C. Zerner, J. Phys. Chem. **96**, 6949 (1992).
105. J. Mavri, H. J. C. Berendsen, and W. F. van Gunsteren, J. Phys. Chem. **97**, 13469 (1993).
106. I. Tuñón, E. Silla, and J. Bertran, J. Phys. Chem. **97**, 5547 (1993).
107. E. C. Meng, P. Cieplak, J. W. Caldwell, and P. A. Kollman, J. Am. Chem. Soc. **116**, 12061 (1994).
108. M. P. Allen and D. J. Tildesley, *Computer Simulation of Liquids* (Clarendon Press, Oxford, 1987).
109. A. H. Juffer and H.J. C. Berendsen, Mol. Phys. **79**, 623 (1993).
110. S. J. Weiner, P. A. Kollman, D. A. Case, U. C. Singh, C. Ghio, G. Alagona, S. Profeta, and P. Weiner, J. Am. Chem. Soc. **106**, 765 (1984).
111. S. J. Weiner, P. A. Kollman, D. T. Nguyen, and D. A. Case, J. Comp. Chem. **7**, 230 (1986).
112. J. Hermans, H. J. C. Berendsen, W. F. van Gunsteren, and J. P. M. Postma, Biopolymers **23**, 1513 (1984).
113. J. Åqvist, W. F. van Gunsteren, M. Leijonmarck, and O. Tapia, J. Mol. Biol. **183**, 461 (1985).